An atomic X-ray absorption fine structure study of the influence of hydrogen chemisorption and support on the electronic structure of supported Pt particles

D.E. Ramaker [a], G.E. van Dorssen [b], B.L. Mojet [b,*] and D.C. Koningsberger [b,**]

[a] *Department of Chemistry and Materials Science Institute, George Washington University, Washington, DC 20052, USA*
[b] *Department of Inorganic Chemistry and Catalysis, Debye Institute, Utrecht University, PO Box 80083, 3508 TB Utrecht, The Netherlands*

The physical principles of atomic XAFS (AXAFS) are presented along with important details on how to isolate the AXAFS contribution from the experimental XAFS data. Intuitive illustrations are given showing how various interactions of the absorber atom with its neighbours influence the AXAFS contribution. Hydrogen chemisorbed on the surface of the supported metal particles is shown to have a strong influence on the amplitude of the Fourier transform AXAFS peak. The effect of the support (with different amounts and types of charge compensating ions (H^+, K^+), different Si/Al ratio and extra-framework Al) on the experimental AXAFS spectra of Pt dispersed in zeolites (LTL,Y) and on flat supports (Al_2O_3–SiO_2, MgO–Al_2O_3) are summarised. It is shown that the essence of the metal–support interaction, as revealed in the AXAFS, is a shift in the ionisation potential of the valence d-orbital electrons brought about by the polarisation induced primarily by the changing charge on the support oxygen atoms.

Keywords: atomic XAFS spectroscopy, supported platinum catalysts, metal–support interaction, Pt electronic structure, hydrogen chemisorption, particle size effects

1. Introduction

Numerous studies have reported enhancements in the specific reaction rates of metal particles for benzene hydrogenation [1,2], propane hydrogenolysis [3,4] and neopentane hydrogenolysis and isomerisation [4–7] on acidic supports compared to neutral supports. These differences were believed to be due to an interaction between the metal particles and the support. The metal–support interaction has been shown not only to alter the catalytic behaviour, but there also are indications that it changes the electronic properties of the supported metal cluster. Several explanations for the metal–support interaction have been proposed in the literature: (i) formation of a metal–proton adduct, with the number of protons determined by the acidity of the support [5,8]; (ii) charge transfer between the metal atoms and the nearest neighbour zeolite oxygen atoms [9–11]; and (iii) polarisation of the metal particles by nearby cations in the support [12,13]. It has been previously indicated [14] that most of these explanations are not based upon a firm experimental basis, and indeed some contradict recent experimental data.

Systematic experiments [15–17] have shown that the catalytic activity and spectroscopic properties of supported noble metal catalysts are greatly affected by the charge compensating cations (H^+, K^+) in LTL zeolite. As the K^+ content of the support increases, the TOF of the metal particles for neopentane hydrogenolysis decreases. At the same time, there is a decrease in the (Pd) XPS binding energy and a shift from linear to bridge bonded CO in the FTIR spectra of Pd and Pt. The XPS and the FTIR results provide a strong indication for a direct influence of the support on the electronic properties of the metal particles. These effects were found to be independent of the metal (Pd or Pt). The turnover frequency (TOF) for conversion of neopentane was also determined for Pt in Y zeolite with different numbers of protons and La^{3+} ions, different Si/Al ratio and with non-framework Al present [14]. As in Pt/LTL, an increase in the Pt TOF was found to be proportional to the number of protons. The TOF of Pt in non-acidic NaLaY zeolite was about 25 times higher than for NaY, which in addition indicates a strong influence of the charge of cations in the zeolite on the TOF of Pt. The 20 times increase in Pt TOF for K-USY compared to NaY was attributed to the higher Si/Al ratio and/or the presence of non-framework Al in K-USY. Pt particles supported on flat supports also experience an influence of the acidity/basicity of the support on the neopentane TOF of platinum. The TOF of Pt/Al_2O_3–SiO_2 is about 500 times higher than on Pt/MgO–Al_2O_3 [18].

In order to investigate the electronic nature of the metal–support interaction, we have developed two new *in situ* techniques in X-ray absorption spectroscopy (XAS) that provide previously unobtainable electronic structure information on supported noble metal catalysts. The first technique utilises the "atomic" X-ray absorption fine structure (AXAFS) in the XAFS data, which results in direct information on the changes in the electronic structure (embedded potential) of the average Pt atom in the cluster [19]. The second technique uses the Pt–adsorbate anti-bonding shape resonances near the X-ray absorption edge, that provide

* Current address: Schuit Institute of Catalysis, Eindhoven University of Technology, PO Box 523, 5600 MB Eindhoven, The Netherlands.
** To whom correspondence should be addressed.

© J.C. Baltzer AG, Science Publishers

insight in the changes in nature of adsorbate bonding to Pt clusters [20]. The AXAFS and shape resonances can be used as new tools to examine changes in the electronic structure of metal clusters, and the resultant changes in the adsorbate–metal bonding, respectively, induced by the metal–support interaction, reduction temperature, and presence of chemisorbed hydrogen. Here, we concentrate on the AXAFS technique. The following article in this issue will deal with the applications of shape resonances in catalysis research.

The recent AXAFS results demonstrate that (i) the charge on a metallic cluster can be monitored with AXAFS with changes as small as 0.05 e (electronic charge) clearly detectable [21], (ii) polarisation effects from ions at a distance of two and three coordination shells from the absorber are clearly visible [22], and (iii) the amplitude and shape of the Fourier transform AXAFS peak directly correlates with the TOF for Pt clusters in zeolites (LTL, Y) [14,17] and on flat supports (Al_2O_3–SiO_2, MgO–Al_2O_3) [18]. This means that the effect of the metal–support interaction is reflected in the AXAFS Fourier transform.

In this paper the fundamental physical principles of AXAFS will be presented along with important details on how to isolate the AXAFS contribution from the experimental XAFS data. Intuitive illustrations will be given showing how various interactions of the absorber atom with its neighbours influence the AXAFS contribution. Two important effects are distinguished: (i) the through-space field effect and (ii) the through-bond inductive effect. It will be shown that hydrogen chemisorbed on the surface of the supported metal particles has a strong influence on the amplitude of the Fourier transform AXAFS peak. This implies that hydrogen has to be removed from the surface of the metal particles before the influence of the support on the electronic structure of the metal particles can be investigated with AXAFS spectroscopy. The effect of the support (with different amounts and types of charge compensating ions (H^+, K^+), different Si/Al ratio and extra-framework Al) on the experimental AXAFS spectra of Pt dispersed in zeolites (LTL,Y) and on flat supports (Al_2O_3–SiO_2, MgO–Al_2O_3) will be summarised and discussed. It will be shown that the essence of the metal–support interaction is a shift in the ionisation potential of the valence d-orbital electrons. This new model for the metal–support interaction will be compared with previously proposed models in the literature.

2. Methods

2.1. Physical principles of atomic XAFS

The total absorption cross section in the extended X-ray absorption fine structure (EXAFS) is normally written as $\mu = \mu_{\text{emb}}(1 + \chi_{\text{EX}})$, with χ_{EX} the EXAFS function. The absorbing embedded atom (i.e., the atom bonded to its environment) accounts for the major part μ_{emb} of the absorption coefficient. The structure in χ_{EX} enables the local geometry

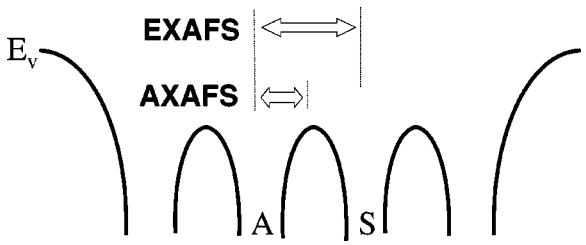

Figure 1. Physical origin of EXAFS and AXAFS in a schematic potential model. A: absorber atom potential; S: scattering atom; and E_{v}: vacuum level.

about the absorbing atom to be determined [23]. Holland et al. [24] and more recently Rehr et al. [25] noted that μ_{emb} is not a totally smooth function, but can also have structure χ_{AX} due to scattering from the periphery of the absorbing atom itself. Thus the atomic cross section of the embedded atom can be expressed as $\mu_{\text{emb}} = \mu_{\text{free}}(1 + \chi_{\text{AX}})$ with μ_{free} the absorption cross section for the free atom in contrast to that for the embedded atom μ_{emb}. The χ_{AX} function called "atomic" XAFS (AXAFS) [19], offers the possibility to obtain electronic structure information utilising a procedure comparable to EXAFS. The two scattering phenomena (AXAFS and EXAFS) are schematically illustrated in figure 1.

The AXAFS represents the change in scattering by the absorbing atom itself relative to the free atom (*vide infra*). This change is due to bonding of the absorbing atom with its environment; consequently any changes in the environment, which changes the electronic charge or structure of the absorbing atom, should be reflected in the AXAFS. AXAFS originates from scattering of photoelectrons in the periphery of the absorber atom itself. The AXAFS contribution introduces an additional oscillation, albeit of longer wavelength because of the smaller distance to the source of scattering. This additional oscillation is normally factored out so that $\mu = \mu_{\text{free}}(1 + \chi_{\text{AX}})(1 + \chi_{\text{EX}})$. In principle, this AXAFS scattering is somewhat larger than normal EXAFS due to the shorter distance and the $1/R^2$ factor out front (see equation (1) [26]). Also, the electron density completely surrounds the absorber atom instead of being concentrated at several lattice sites around the absorber. On the other hand, the AXAFS scattering is short ranged in k, because it arises primarily from scattering by the deep valence electrons rather than the core electrons as in EXAFS. This makes the peak in the FT-AXAFS wider and generally smaller in magnitude than the regular EXAFS scattering.

In order to outline the scattering process, a description of the potential surrounding the absorber atom is necessary. The well-known muffin-tin approximation can be used to approximate the embedded atom potential. As illustrated in figure 2, the muffin-tin approximation "clips" the exact potential at the muffin-tin radius R_{mt} and sets it equal to the interstitial potential V_{int} [19]. Inside R_{mt} the potential is assumed to be spherical, outside it is assumed to be flat and zero (i.e., no forces are exerted on the particle in the interstitial region). V_{int} is determined by averaging the potential at R_{mt} of all the atoms in the cluster, this

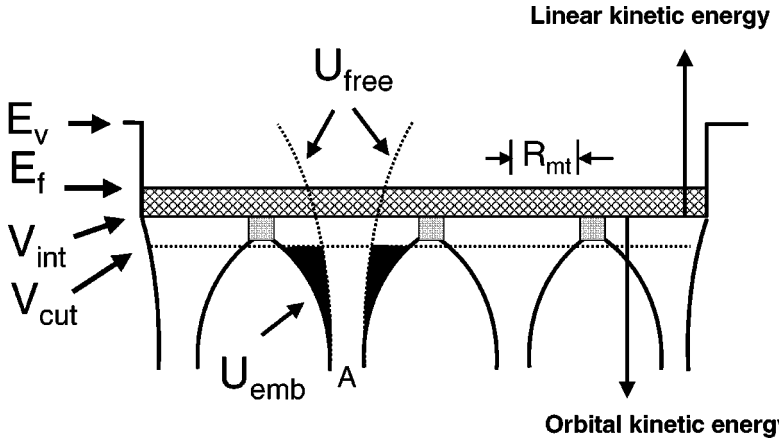

Figure 2. Illustration of the muffin-tin approximation to the interatomic potentials showing locations of $R_{\rm mt}$, $V_{\rm int}$ and $E_{\rm f}$. The shape and intensity of the Fourier transform of the AXAFS is determined by the black shaded area between $U_{\rm emb}$ and $U_{\rm free}$ and below $V_{\rm cut}$ as defined in the text. Maximum scattering occurs when the linear kinetic energy of the photoelectron is equal to the orbital kinetic energy of the electron scatterer.

determines the zero of energy or the effective bottom of the conduction or itinerant band.

The AXAFS is best reflected in the Fourier transform (FT) of $\chi_{\rm AX}$, which produces the first peak at approximately 1/2 the first-shell bond length. $\chi_{\rm AX}$ can be expressed mathematically in a first distorted wave Born approximation [19] and using the muffin-tin approximation as

$$\chi_{\rm AX}(k) \approx -(2m/(kh))\mathrm{Im}\int \mathrm{e}^{2\mathrm{i}kr+2\mathrm{i}\delta}\Delta U\,\mathrm{d}r, \qquad (1)$$

where $\Delta U = U_{\rm emb} - U_{\rm free}$ with $U_{\rm emb}$ the embedded atom potential, $U_{\rm free}$ the truncated free atom potential. In this paper, potentials that are a function of the distance from the absorber are denoted by U. Lines with constant potential values are given by V. The free atom potential ($U_{\rm free}$) reflects the electron distribution in the free atom. The embedded potential ($U_{\rm emb}$) reflects the electron distribution after embedding the free atom into its chemical environment and allowing interaction with its neighbours.

A phase corrected and k weighted Fourier transform of $\chi_{\rm AX}(k)$ leads to [19]

$$\left|\mathrm{FT}\left(k\mathrm{e}^{-2\mathrm{i}\delta}\chi_{\rm AX}\right)\right| \approx \Delta U\Gamma, \qquad (2)$$

with Γ a broadening function due to the limited Fourier transform range. Equation (2) then reveals that the FT-AXAFS directly reflects the change in the chemical environment. More specifically, the shape and intensity of the |FT| can be represented by the black area between $U_{\rm free}$ and $U_{\rm emb}$ and below $V_{\rm cut}$ ($V_{\rm cut} = 2V_{\rm int} + |E_{\rm f}|$), as illustrated in figure 2.

The scattering of the photoelectron by an electron in an orbital is primarily resonant, which implies that scattering occurs if the kinetic energy of the photoelectron is equal to the kinetic energy of the bound electrons doing the scattering. Going upward above $E_{\rm f}$ in figure 2, the linear kinetic energy of the photoelectron increases, going downward below $V_{\rm int}$, the orbital kinetic energy of the valence electrons localised on a single atom increases. The photoelectron at the absorption edge already has kinetic energy equal to $E_{\rm f}$ minus $V_{\rm int}$. The electrons in the conduction band are not effective for scattering because they have kinetic energy well below that of this photoelectron even at threshold. Moreover, the electrons in states above $V_{\rm cut}$ have insufficient orbital kinetic energy. Thus only electrons in states below $V_{\rm cut}$ (i.e., with higher binding energy) will be effective at scattering photoelectrons with kinetic energy near or well above threshold. In summary, only the *deeper localised* valence band electrons give rise to AXAFS scattering.

2.2. The field and inductive interactions

Obviously the AXAFS will change by either altering $U_{\rm emb}$ or $V_{\rm cut}$ (the latter directly determined by the position and width of the itinerant conduction band). A change in the nature or number of bonds around the absorber atom will definitely change these two properties of the absorber atom, and the AXAFS should change accordingly. We can straightforwardly predict that an increase in the number of bonds about an absorber atom will pull down $U_{\rm emb}$ (i.e., increase the "roll-over" of $U_{\rm emb}$) so that the AXAFS will increase. Further, a change in the nature of the bond, say decreasing its covalent character, will decrease the AXAFS. This is because a decrease in the covalent nature will limit the "roll-over" in $U_{\rm emb}$. Finally, the removal of an electron from the absorber atom (ionisation) will result in an increase in the AXAFS. This is perhaps not obvious, because one might expect the fewer electrons remaining on the absorber atom to scatter less. However, the removed electron is generally taken from the Fermi level, and this electron was not an effective scatterer anyway; but the removal of this electron causes all of the other electrons to shift to higher binding energy causing them to become more effective scatterers. This shift is similar to the increase in ionisation potential of an atom as its charge is increased. This explains the change in AXAFS with a Pt electrode as experimentally observed by O'Grady et al. [21].

Actually, many more subtle long-range effects can be seen in the AXAFS, and this is critical to application of

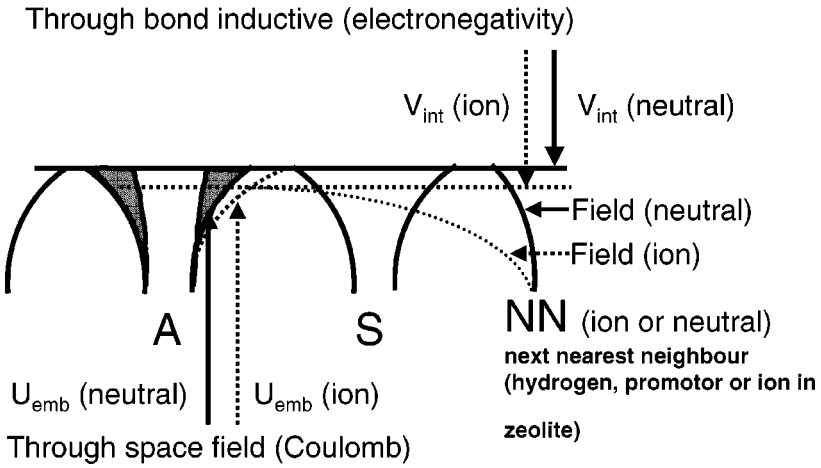

Figure 3. Effect of ionicity or charge of next nearest neighbours on position of V_{int} and U_{emb}.

AXAFS to examine the metal–support interaction. In the muffin-tin model used to describe AXAFS, polarisation by more distant atoms can modify the absorber atom in the same two ways as described above: (i) by the direct overlap of the nearby atom potentials, altering U_{emb}, the *through-space field effect* [27,28], or (ii) by affecting the average V_{int} and V_{cut}, which will be referred to as the *through-bond inductive effect* [27,28]. This is appropriate because if a neighbouring atom is highly electronegative, V_{int} will be more negative, which means that more electrons will be delocalised into the interstitial region, exactly the nature of the inductive effect. In figure 3 these two interactions are illustrated by the effect of a neutral or ion (long-range Coulomb) potential of a next nearest neighbour atom on a Pt absorber atom. The influence of the charge of the neighbouring atom is to pull down (increase the "roll" over of) U_{emb}, which describes the through-space field effect. The influence of the higher electronegativity is to lower the position of V_{int}, which delocalises electron density from within the platinum cluster to the interstitial region between the platinum and oxygen. The exact nature in which these two potentials change via the metal–support interaction will be considered in detail in section 3.

3. Isolation of AXAFS and applications to study supported metal catalysts

3.1. Isolation of AXAFS

3.1.1. Background subtraction

As discussed in [26], the first step in isolating the AXAFS from the experimental data is removal of the pre-edge background. Then the edge position is chosen (at the inflection point of the absorption edge, or at 0.6 of the total step height of the edge). The post-edge background removal is the most controversial and difficult, usually accomplished by spline smoothing [26]. New criteria for removing this background are required for isolating the AXAFS. The long wavelength oscillations in AXAFS make extraction of χ_{AX} from the full μ somewhat problematical. Double-electron excitations are also present [29,30], which in addition cause structure of long wavelength; albeit with irregular wavelength, making a precise separation of these contributions somewhat difficult.

Figure 4 illustrates the background subtraction problem. We have used the normal cubic-spline to fit the atomic background [26,31]. Three primary contributions appear in the Fourier transform between $0 < R < 2.8$ Å: (i) the free-atom contribution which we have shown elsewhere [30] to consist of double-electron excitations (DEE) and the Ramsauer–Townsend resonance (RTR), peaking between $0 < R < 0.5$ Å, (ii) the true AXAFS feature between $0.5 < R < 1.2$ Å, and (iii) the first-shell Pt–Pt EXAFS around $R = 2.3$ Å. The objective is to leave χ_{free} in the background and χ_{AX} in the full χ. Figure 4 shows the effect of three different levels of spline smoothing used for the background subtraction for a Pt/K-LTL catalyst [19]. In figure 4(a)–(c), the smoothing parameter is lowered in such a way that in: (a) a considerable amount of the free-atom absorption is left in the χ data, which is visible between $0 < R < 0.5$ Å in the Fourier transform, and tailing off to higher distances; (b) almost all free atom scattering is removed, but the AXAFS signal at $R = 1$ Å is still present in χ; (c) all intensity at low R-values in the Fourier transform is removed from χ following the background criteria used before the existence of AXAFS was really established. The optimum background subtraction is to retain the AXAFS in the Fourier transform of χ, as shown in figure 4(b). Three criteria are now used to determine a consistent background:

(a) Diminish the free atom contribution between $0 < R < 0.5$ Å to essentially zero. Check whether the RTR and DEE fully remain in the background by directly examining the background.

(b) Leave the amplitude of the EXAFS peaks unreduced as much as possible.

(c) Check this procedure both in k^1 and k^3 weighting for different k-ranges, including low k-values (e.g., k down

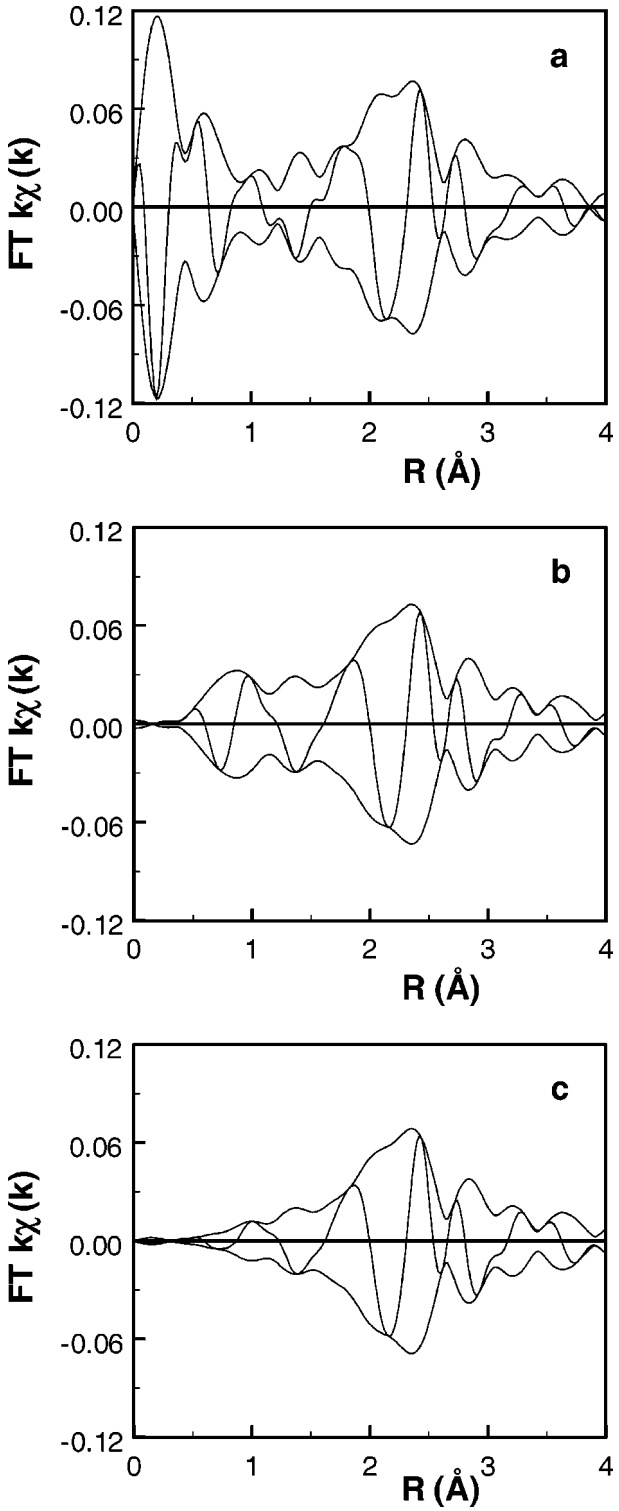

Figure 4. Fourier transform (k^1, $3.0 < k < 13.5$ Å^{-1}) of experimental χ data from Pt/LTL (K/Al = 0.96) after three levels of background smoothing [19]: (a) all contributions left in the χ; (b) RTR and DEE removed; and (c) RT, DEE and AXAFS removed.

to 1.5 Å^{-1}). The last criterion is important to ensure that very little EXAFS signal is removed from the data.

Previously, it was often required to remove about 10% of the intensity of the first-shell EXAFS peak in order to eliminate the AXAFS peak (figure 4(c)). Now we need only a 1–2% reduction in this first EXAFS peak to eliminate the free-atom contribution, but keep the AXAFS. The AXAFS peak remaining at small R is the difference between the scattering for the embedded atom relative to the free atom as discussed above.

3.1.2. Separation of AXAFS from EXAFS data

In order to compare the AXAFS peaks in different systems or under different experimental conditions, it is necessary to separate the AXAFS from the EXAFS data. The Fourier transform of the EXAFS contribution will tail into the AXAFS peak; especially, when first-shell EXAFS contributions have co-ordination distances between $1.5 < R <$ 2.0 Å. This causes interference, which actually can artificially reduce the amplitude of the AXAFS peak as observed in the Fourier transform. An example of the separation of the AXAFS data for a Pt/γ-Al_2O_3 catalysts (reduced at 573 K, evacuated at 573 K, measured at 100 K) [32] is presented in figure 5. The raw EXAFS data are shown in figure 5(a) (solid line). The first-shell contributions consist of a Pt–Pt and a Pt–O peak in a normal (not phase) corrected Fourier transform at 2.3 and around 1.6 Å, respectively (see figure 5(b) (solid line)). The first-shell contributions (Pt–Pt and Pt–O) were fitted in R-space (see figure 5(b) (dotted line)). The difference file technique was used [26] to carry out the fit procedure. The Fourier transform of the resulting difference file (raw data minus calculated Pt–Pt) and the Pt–O contribution are displayed in figure 5(c), with solid and dotted lines, respectively. It was possible to fit the imaginary part and amplitude of the difference file between $1.6 < R < 3.2$ Å. The differences at low R are due to the presence of the AXAFS. A strong overlap exists between the Pt–O contribution and the AXAFS peak. Subtracting the calculated Pt–Pt and Pt–O contribution from the raw data gives a difference file, which contains the AXAFS and higher-shell contributions. The Fourier transform of this difference file is plotted in figure 5(d). It can be seen that the AXAFS peak is isolated. The AXAFS oscillations can now be obtained by applying an inverse Fourier transform from $0 < R < 1.6$ Å. The AXAFS oscillations are shown in figure 5(a) (dotted line). The AXAFS oscillations have a long wavelength and decrease rapidly with increasing values of k.

3.2. Effect of hydrogen chemisorption

Chemisorption of hydrogen leads to a change in the electronic structure of the surface and bulk atoms constituting the platinum particles. The isolated experimental AXAFS data show this effect averaged over all atoms present in the metal particles. Figure 6 compares the isolated AXAFS of the Pt/γ-Al_2O_3 catalysts as given above without (solid line) and with (dotted line) chemisorbed hydrogen [32]. It can clearly be seen that hydrogen chemisorption increases the amplitude of the AXAFS peak below 1.0 Å and decreases

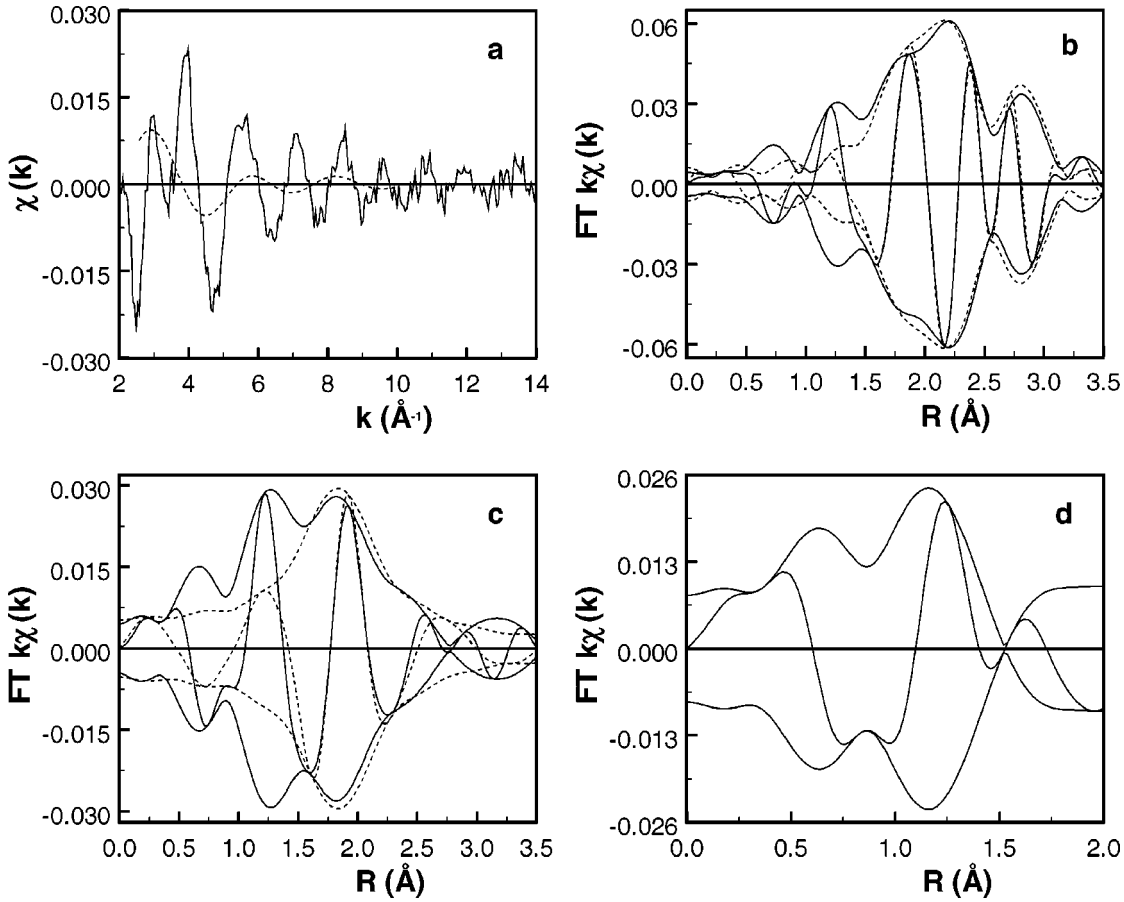

Figure 5. XAFS analysis of a Pt/γ-Al_2O_3 catalysts reduced at 573 K, evacuated at 573 K, and measured at 100 K: (a) raw EXAFS data (——) and isolated AXAFS (- - -) (see text); (b) Fourier transforms (k^1, $2.5 < k < 11$ Å^{-1}) of raw data (——) and best fit (- - -) (k^1, $2.5 < k < 11$ Å^{-1}, $1.6 < R < 3.1$ Å); (c) Fourier transforms (k^1, $2.5 < k < 11$ Å^{-1}) of Pt–O phase corrected difference file (raw data minus first-shell Pt–Pt contribution) (——) and Pt–O fit (- - -); and (d) Fourier transform (k^1, $2.5 < k < 10$ Å^{-1}) of difference file (raw data minus first-shell Pt–Pt and Pt–O contribution) representing the AXAFS contribution. Fourier filtering ($0 < R < 1.9$ Å) of this difference file produces the AXAFS oscillations as given in (a) with (- - -).

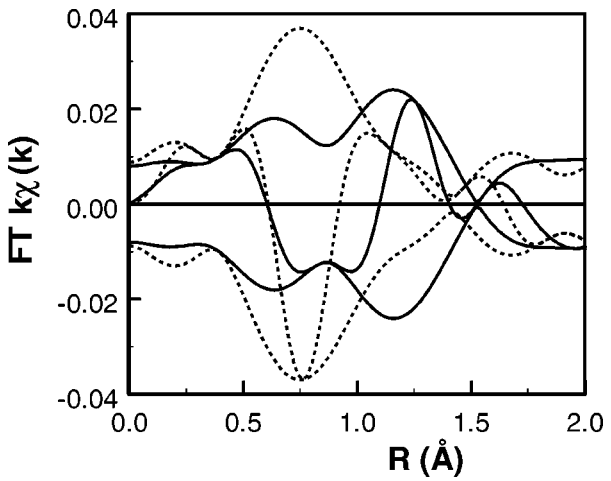

Figure 6. Fourier transform (k^1, $2.5 < k < 10$ Å^{-1}) of isolated AXAFS for the Pt/γ-Al_2O_3 catalysts reduced at 573 K with chemisorbed hydrogen (- - -) and after subsequent evacuation at 573 K (——).

it above 1.0 Å (i.e., it changes the position of the centroid to lower values of R).

3.3. Metal–support interaction

The intensity and shape of the Fourier transform of the AXAFS data of supported Pt particles dispersed in zeolites (LTL, Y) and on flat supports (Al_2O_3–SiO_2, MgO–Al_2O_3) is also strongly dependent on the amounts and types of charge compensating ions (H^+, K^+), Si/Al ratio and extra-framework Al [14,17,18]. Figure 7 summarises the experimental results from these studies. Figure 7(a) gives the Fourier transforms of the AXAFS data for Pt/LTL catalysts with different K/Al molar ratio of the LTL zeolite [17]. The Fourier transform of the isolated AXAFS peak of Pt/NaY and Pt/H-USY is displayed in figure 7(b). Here the effect of a different Si/Al ratio and extra-framework Al was studied [14]. The effect of a different acidity/basicity of a flat support on the Pt particles was investigated for Pt/Al_2O_3–SiO_2 and Pt/MgO–Al_2O_3. The Fourier transform of the isolated AXAFS data for these samples is shown in figure 7(c).

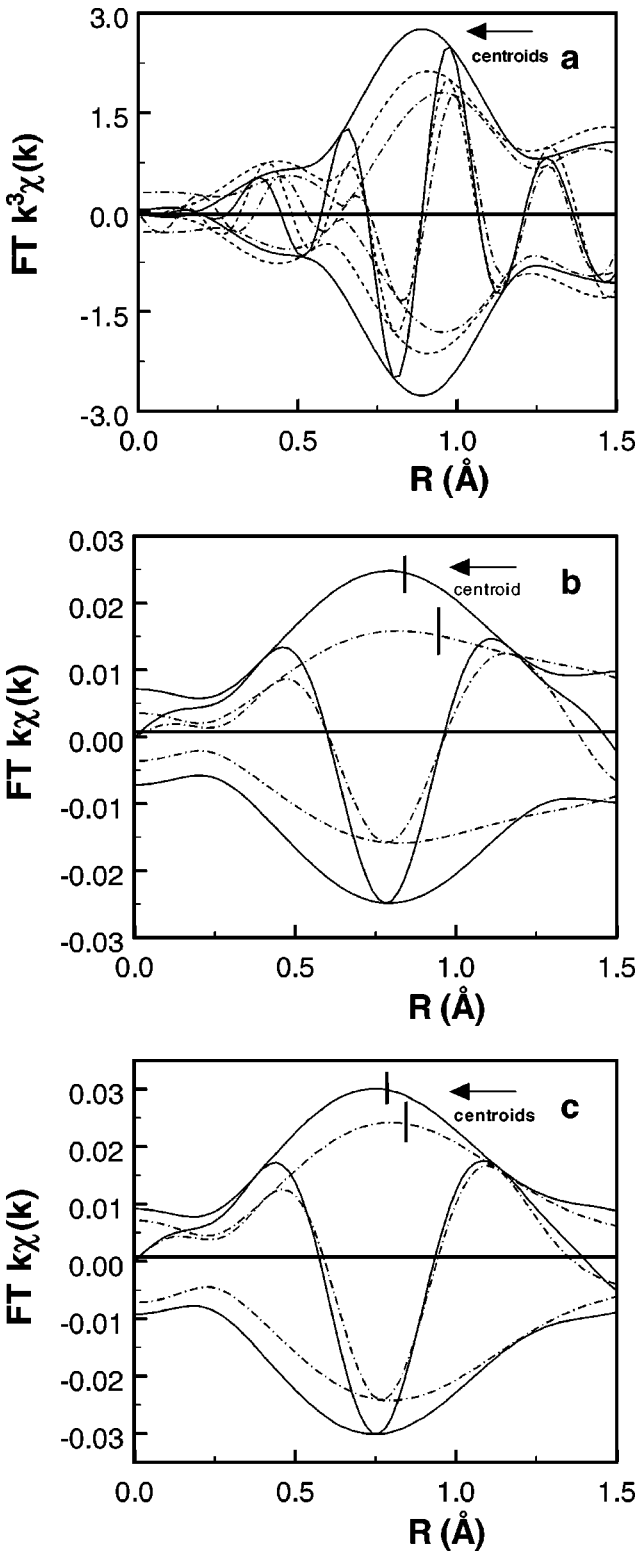

Figure 7. Influence on support properties on Fourier transform AXAFS peak: (a) Fourier transform (k^3, $3.0 < k < 13$ Å^{-1}) of the AXAFS data for Pt/LTL (——) K/Al = 0.63, (- - -) K/Al = 0.96, (·····) K/Al = 1.25 (data obtained from [17]); (b) Fourier transform (k^1, $2.5 < k < 8$ Å^{-1}) of the isolated AXAFS of Pt/H-USY (——) and Pt/Na-Y (·····) (data obtained from [15]); and (c) Fourier transform (k^1, $2.5 < k < 8$ Å^{-1}) of the isolated AXAFS of Pt/SiO_2–Al_2O_3 (——) and Pt/SiO_2–MgO (·····) (data obtained from [18]).

4. Discussion

4.1. Isolation of AXAFS

The results presented in section 3.1 make clear that a very careful and systematic background subtraction procedure is necessary before the AXAFS and EXAFS signals are fully separated from the atomic background and double-electron excitations. The described procedure of monitoring, as a function of the smooth parameter (SM), the full appearance of the double-electron excitations in the background signal allows for a more objective approach compared to that used in the past for the separation of the EXAFS from the background signal. Moreover, it is demonstrated that the R-space fitting technique makes it possible to further isolate the AXAFS data from the first-shell Pt–Pt and Pt–O EXAFS contributions. The use of non-isolated AXAFS data for monitoring metal–support effects can lead to problems, since the first-shell Pt–Pt and Pt–O Fourier transform EXAFS data have tails in the R region of the AXAFS peak. The isolation of the AXAFS data as described in this paper is a prerequisite for the use of AXAFS spectroscopy to study the influence of the support and adsorbates on the electronic structure of supported metal particles.

4.2. Effect of hydrogen chemisorption

Hydrogen chemisorption on the surface of the supported metal particles leads to an average net increase in the AXAFS signal (see figure 6). Moreover, a large shift to lower values of R is observed for the centroid of the AXAFS peak. This can be explained by realising that the effect of hydrogen chemisorption is averaged over all atoms present in the metal cluster. The through-space field effect on the Pt surface atoms will increase the amplitude of the FT-AXAFS peak. However, it is possible that the bulk and interfacial Pt atoms exhibit a larger inductive effect than the Pt surface atoms. This will lower the V_{int} (or V_{cut}) value in the particle, which leads to a shift of the centroid of the Fourier transform AXAFS peak to lower values of R. Preliminary results of AXAFS calulations using the FEFF7 code indeed show the occurrence of these effects.

4.3. A new model for metal–support interaction

The results presented here and those published previously [14,17,18] indicate that AXAFS is a powerful new tool for obtaining unprecedented detail on the nature of the metal–support interaction. The results of preliminary calulations with the FEFF7 code by simply changing the charge on the support O atoms reproduce remarkably well the experimentally observed changes in the AXAFS data as a function of the support properties.

The new model is presented in figure 8 (a) and (b). In figure 8(a), the field effect of a neutral O "support" atom

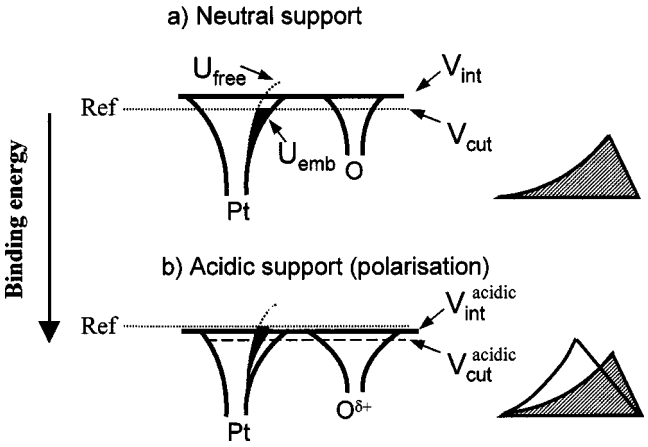

Figure 8. Schematic potential curves for the interaction of Pt with a neutral (δ^0) oxygen and an oxygen with less negative charge (δ^+). Note that the O atom with the δ^+ charged is shown with a longer range Coulomb potential at an higher binding energy (more negative potential). The hatched areas on the right side illustrate the expected FT of the AXAFS for the neutral support. The dark shaded area is proportional to $U_{\text{free}} - U_{\text{emb}}$ for the neutral support. Its energy position is taken as a reference (indicated by Ref). The transparent area reflects the ΔU area for the acidic support: its intensity is higher and the centroid is shifted to lower R due to increased "roll-over" of U_{emb} and lowering of V_{cut}.

is shown. For the neutral O atom, the field effect is very short ranged, so no polarisation of the cluster occurs. The black area represents ΔU, the difference between U_{free} and U_{emb}, which represents the FT-AXAFS. The position of V_{cut} is taken as a reference (REF) for the energy scale. The hatched area on the right side of figure 8(a) is a "blow-up" of the black area on the left and represents the expected amplitude and shape of the FT-AXAFS. As positive charge is added to the oxygen in figure 8(b) (as occurs for an acidic support), the field effect induced by the extra positive charge now becomes longer range so that Pt atoms across the cluster each feel a different field. Since the cluster may be partially metallic, charge may flow toward the support O until the potential across the cluster is the same. The final potential of the cluster is "pulled down" in comparison to the reference value defined in figure 8(a). This leads to higher amplitude of FT-AXAFS and a shift of the centroid of this peak to lower R values.

The pulled down potential results in a shift of the valence d-orbitals to higher binding energies (more negative potential), thus leading to a change in electronic properties of the Pt particles. Consequently, the new model predicts that one of the most important aspects of the metal–support interaction is a change in the ionisation potential of the Pt particle brought about by polarisation induced by by the support oxygen ions. The FEFF7 calculations not shown here indicate that the electronic properties of the platinum surface atoms representing the catalytically active sites are directly influenced by a change in the charge density on the support oxygen ions. This is the essence of the metal–support interaction: a change in catalytic properties of the supported metal particles directly induced by the support.

As mentioned in section 1, several previous models have been proposed for the metal–support interaction. One model proposes the formation of a metal–proton adduct [5,8] to account for electron-deficient metal particles observed in acidic zeolites. The protons are thought to be delocalised over the metal particle and withdraw electron density from the surface atoms. However, such adducts cannot account for an increase in electron density for metal particles on alkaline supports. Alternatively, it is suggested that the electronegativity of the support oxygen atoms increases with rising zeolite alkalinity [10,11]. Charge transfer [9] between the support oxygen atoms and the close-by metal particles is thought to cause higher electron density on the metal particles in alkaline zeolites. These two models are similar in that they both propose a transfer of electron density from (or to) the metal particles due to the metal–support interaction. The only difference between the models is that in the former the metal transfers electron density to the support protons, while in the latter the transfer is thought to occur between the metal and the oxide ions. A third explanation is based on the polarisation of a metal cluster by nearby cations [12,13]. Calculations indicate that metal atoms near cations attract electrons, thus resulting in electron-deficient metal atoms situated at the opposite side of the cluster. In this model, there is no net change in the total electron density of the cluster, however polarisation of the electron density leaves those atoms that participate in the catalysis electron deficient.

As discussed in [14], a real charge transfer of the metal particle to the support would leave the centroid of the FT-AXAFS peak unchanged, whereas a shift is observed experimentally. This fact, and other important arguments put forward by Ponec and Bond [33], make the charge transfer model very unrealistic. Also polarisation by cations is thought not very likely to occur. As discussed in [14], polarisation of the metal particle can indeed occur, the magnitude depending on the particle morphology. However, in the current model, this polarisation is not due to the presence of cations, but induced by the support oxygen ions.

The current model is also consistent with other data. The shift to higher binding energy of the valence orbitals for platinum particles on acidic supports, as deduced from our AXAFS study, is entirely consistent with the IR data for CO adsorbed on Pt/LTL. The shift increases the energy difference between the interacting d-orbital and the CO $2\pi^*$ orbital, which lowers the back-donation of platinum to CO. The FTIR CO data show an increased ratio of linear/bridged bonded CO in the case of an acidic support, consistent with the greater difficulty for the charge transfer required in the bridged CO configuration [34]. Finally Pd 3d XPS data reveals an increased binding energy for palladium particles on acidic supports. The polarisation of the palladium electron charge towards the interfacial region, induced by a less negative oxygen charge will indeed result in less screening of the core hole in the XPS final state. This

causes a larger binding energy of the valence electrons of metal particles on acidic supports. All of this data point to a cluster on acidic supports acting as if it were less metallic, even though no net charge has been removed from the cluster. This is consistent with an increased binding energy of the d-valence electrons [34]. The subsequent paper will present an analysis of the Pt–H shape resonances, which reveal a similar reduction in charge transfer to the H atoms chemisorbed on the surface of platinum particles dispersed on acidic supports.

5. Conclusions

AXAFS has proven to be a powerful new tool to examine the electronic structure of supported noble metal clusters. It suggests strongly that the metal–support interaction results primarily from the "through-space" field interaction, which increases the binding energy of the valence electrons of metal particles dispersed on acidic supports. Further work on larger clusters supported on amorphous supports is in progress to deeper study the turn off of this metal–support interaction. The investigation towards the role of promoter atoms is also under way. Finally, much more work is required for other supported metals, oxides and sulfides to determine the general applicability of the findings presented here. Nevertheless, it is anticipated that the results and ideas presented in this work will not change radically for these other systems.

Acknowledgement

The authors like to thank the stimulating discussions and encouragement of Dr. J.T. Miller (AMOCO Research Centre, Naperville, USA). They are thankful for the help and stimulating interest of the scientific staff of beamline BM29 of the ESRF (Grenoble, France) and beamline 9.2 of the SRS (Daresbury, UK).

References

[1] F. Figueras, J.R. Gomez and M. Primet, Adv. Chem. Ser. 121 (1973) 480.
[2] S.D. Lin and M.A. Vannice, J. Catal. 143 (1993) 539.
[3] M. Vaarkamp, J.T. Miller, F.S. Modica, G.S. Lane and D.C. Koningsberger, in: *Proc. 10th Int. Congr. Catal.*, Budapest (1992) p. 809.
[4] J.T. Miller, F.S. Modica, B.L. Meyers and D.C. Koningsberger, Prep. ACS Div. Petr. Chem. 38 (1993) 825.
[5] Z. Karpinski, S.N. Gandhi and W.M.H. Sachtler, J. Catal. 141 (1993) 337.
[6] S.T. Homeyer, Z. Harpinski and W.M.H. Sachtler, J. Catal. 123 (1990) 60.
[7] R.A. Dalla Betta and M. Boudart, in: *Proc. 5th Int. Congr. Catal.*, Vol. 2, ed. J.W. Hightower (North Holland, Amsterdam, 1973) p. 1329.
[8] Z. Zhang, T.T. Wong and W.M.H. Sachtler, J. Catal. 128 (1991) 13.
[9] G. Larsen and G.L. Haller, Catal. Lett. 3 (1989) 103.
[10] A. de Mallmann and D. Barthomeuf, J. Chem. Phys. 87 (1990) 535.
[11] A. de Mallmann and D. Barthomeuf, Stud. Surf. Sci. Catal. 46 (1989) 429.
[12] A.P. Jansen and R.A. van Santen, J. Phys. Chem. 94 (1990) 6764.
[13] E. Sanchez-Marcos, A.P.J. Jansen and R.A. van Santen, Chem. Phys. Lett. 16 (1990) 399.
[14] D.C. Koningsberger, J. de Graaf, B.L. Mojet, J.T. Miller and D.E. Ramaker, Appl. Catal. 191 (2000) 205.
[15] B.L. Mojet, M.J. Kappers, J.C. Meyers, J.W. Niemantsverdriet, J.T. Miller, F.S. Modica and D.C. Koningsberger, Stud. Surf. Sci. Catal. 84 (1994) 909.
[16] B.L. Mojet, M.J. Kappers, J.T. Miller and D.C. Koningsberger, Stud. Surf. Sci. Catal. 101 (1996) 1165.
[17] B.L. Mojet, J.T. Miller, D.E. Ramaker and D.C. Koningsberger, J. Catal. 186 (1999) 373.
[18] D.C. Koningberger, M.K. Oudenhuijzen, D.E. Ramaker and J.T. Miller, Proceedings ICC12, accepted.
[19] D.E. Ramaker, B.L. Mojet, W.E. O'Grady and D.C. Koningsberger, J. Phys. Condens. Matter. 10 (1998) 1.
[20] D.E. Ramaker, B.L. Mojet, M.T. Garriga Oostenbrink, J.T. Miller and D.C. Koningsberger, J. Phys. Chem. Chem. Phys. 1 (1999) 2293.
[21] W.E. O'Grady and D.E. Ramaker, Electrochim. Acta 44 (1998) 1283.
[22] D.E. Ramaker, X. Qian and W.E. O'Grady, Chem. Phys. Lett. 299 (1999) 221.
[23] D.C. Koningsberger and R. Prins, in: *X-ray Absorption: Principles, Applications and Techniques of MXAFS, SEXAFS and XANES*, eds. D.C. Koningsberger and R. Prins (Wiley, New York, 1988).
[24] B.W. Holland, J.B. Pendry, R.F. Pettifer and J.J. Bordas, Physic. C 11 (1978) 633.
[25] J.J. Rehr, C.H. Booth, F. Bridges and S.I. Zabinsky, Phys. Rev. B 49 (1994) 12347.
[26] D.C. Koningsberger, B.L. Mojet, G.E. van Dorssen and D.E. Ramaker, Topics Catal. 10 (2000) 143.
[27] R.T. Morrison and R.N. Boyd, *Organic Chemistry*, 5th Ed. (Allyn & Bacon, London, 1987).
[28] W.F. Reynolds, J. Chem. Soc. Perkins II 1980 (1980) 985.
[29] A. Philliponi and A. Di Cicco, Phys. Rev. B 53 (1996) 9466.
[30] G.E. van Dorssen, D.E. Ramaker and D.C. Koningsberger, Phys. Rev. B, submitted.
[31] J.W. Cook, Jr. and D.E. Sayers, J. Appl. Phys. 52 (1981) 5024.
[32] G.E. van Dorssen, Ph.D. thesis, Utrecht University (1999).
[33] V. Ponec and G.C. Bond, *Catalysis by Metals and Alloys*, Studies in Surface Science and Catalysis, Vol. 95 (Elsevier, Amsterdam, 1995) p. 234.
[34] R.A. van Santen, J. Chem. Soc. Faraday Trans. I 83 (1987) 1915.